Magnetic properties and magnetic phase diagram of the frustrated $Co_{1-x}Fe_xPt_3$ compounds

T. H. Kim,* M. C. Cadeville, A. Dinia, and V. Pierron-Bohnes
Groupe d'Etudes des Matériaux Métalliques, Institut de Physique et Chimie des Matériaux, UMR 0046 CNRS-Université Louis Pasteur, 23 rue du Loess, F-67037 Strasbourg, France

H. Rakoto
Service National des Champs Magnétiques Pulsés, UMS 819 CNRS–Université Paul Sabatier and INSA de Toulouse, INSA Complexe Scientifique de Rangueil, 31077 Toulouse-Cedex, France
(Received 1 March 1996)

The investigation of the magnetic properties of the pseudobinary $Co_{1-x}Fe_xPt_3$ $L1_2$ ordered compounds resulting from alloying the ferromagnet $CoPt_3$ and the frustrated antiferromagnet $FePt_3$ is reported. dc susceptibilities and zero field cooled and field cooled magnetizations as a function of temperature and field (0–35 T) have been investigated. On the Co-rich side ($x<0.6$), the compounds display a long-range ferromagnetic order characterized by the occurrence of two reentrant spin-glass phases (or mixed magnetic phases) at low temperature and magnetic field starting at very low iron concentration. This ferromagnetic region is closed by a multicritical point located around $x=0.55$ and $T=120$ K. On the iron-rich side, an antiferromagnetic region with two antiferromagnetic $[\frac{1}{2}\frac{1}{2}0]$ and $[\frac{1}{2}00]$ structures is observed for $1\geqslant x>0.8$. Beyond 0.8 the basic antiferromagnetic order $[\frac{1}{2}\frac{1}{2}0]$ changes progressively into a spin-glass ordering and the less stable one $[\frac{1}{2}00]$ persists at low temperature up to Fe concentrations as high as 0.6. Although the complex behavior of the iron-rich side in the intermediate region is not totally elucidated, a tentative phase diagram is proposed and discussed comparatively with the previously determined (Fe-Mn)Pt_3 and (Co-Mn)Pt_3 phase diagrams. The occurrence of a spin-glass phase that separates the long-range ferromagnetic region from the antiferromagnetic one is specific to the (Co-Fe)Pt_3 system in agreement with theoretical models. The (Co-Fe)Pt_3 appears as the most frustrated among the three systems considered. [S0163-1829(96)08129-5]

I. INTRODUCTION

This investigation of the magnetic properties and magnetic phase diagram of the pseudobinary (Co-Fe)Pt_3 system closes the determination of the magnetic phase diagrams between the three binary compounds, namely, the ferromagnetic $CoPt_3$ and $MnPt_3$ and the antiferromagnetic $FePt_3$. The (Fe-Mn)Pt_3 system was investigated in 1985 by Schreiner *et al.*,[1] whereas we published recently a detailed investigation of the (Co-Mn)Pt_3 system.[2] In such ordered $(M\text{-}M')Pt_3$ structures, the M and M' $3d$ transition metals that are mainly responsible for the magnetism are in the position of second nearest neighbors, occupying the corners of the fcc cubic lattice, having 12 Pt atoms in their first neighbor shell. Thus from the point of view of magnetic interactions, the magnetic properties and the magnetic phase diagrams mainly result from the competition between the three predominant direct magnetic exchange interactions J^{2nd}_{MM}, $J^{2nd}_{M'M'}$, and $J^{2nd}_{MM'}$. Whereas the signs of the homoatomic interactions are known from the properties of binary compounds, the sign of the heteroatomic interactions is *a priori* unknown, but it could be deduced from the shape of the magnetic phase diagram. For example, in the case of the (Co-Mn)Pt_3 system where both homoatomic interactions are ferromagnetic, the occurrence of reentrant spin-glass phases at low temperature can be clearly assigned to the presence of a random mean field exchange interaction originated by the negative sign of the Co-Mn interaction. The situation is more complex in ternary phases with iron as $FePt_3$ develops two frustrated antiferromagnetic structures along the $[\frac{1}{2}\ \frac{1}{2}0]$ and $[\frac{1}{2}00]$ directions.[3] The (Mn-Fe)Pt_3 and (Co-Fe)Pt_3 systems will be frustated by nature as, on average, the homoatomic interactions of the binary compounds are different in sign, but the sign and the strength of the heteroatomic interaction may enhance or not the frustrated character. We shall show that information on the sign of the Co-Fe interaction can be deduced from the magnetic properties of the ternary system.

This paper is organized as follows. The second section is devoted to metallurgy. It concerns the elaboration of the ordered phases via the investigation of their ordering kinetics, and their chemical, structural, and microstructural characterization through chemical analysis, x-ray diffraction (XRD), and transmission electron microscopy (TEM). All these points are very important as the magnetic properties are strongly dependent on the degree of order and on the departures from stoichiometry. The study of the magnetic properties will be presented in Sec. III. After a rapid description of the equipment used and a survey of the magnetic behavior over the whole concentration range in Sec. III A, the detailed results will be presented in Secs. III B and III C. Section III B will be devoted to alloys that display a long-range ferromagnetic behavior, namely, a Curie temperature. It concerns the iron concentration range of $0\leqslant x<0.6$. The results obtained on the antiferromagnetic iron-rich side including the occurrence of a spin-glass-like region will be presented and discussed in Sec. III C. We will begin this section by a recall of the magnetic properties of $FePt_3$ investigated by Bacon and Crangle through neutron diffraction[3] and by pre-

 © 1996 The American Physical Society

senting our own results on the binary compound. Such data are absolutely necessary to describe the magnetic behavior of the ternary phases on the iron-rich side. Section IV is a general discussion of the (Co-Fe)Pt_3 phase diagram in the frame of various theoretical approaches, including a comparison with the phase diagrams of the other two (Mn-Fe)Pt_3 and (Mn-Co)Pt_3 systems.

II. METALLURGY

Pure 99.99% Co, Fe, and Pt metals were arc melted together under argon atmosphere on a water-cooled copper boat. The process was repeated several times to assure a good homogeneity. The weight losses during the melting were negligible.

Chemical analyses using the induction coupled plasma (ICP) method were performed on most as-cast samples. They yield Co, Fe, and Pt concentrations in agreement with the nominal ones within the error bar, i.e., $x_{Pt}=0.75\pm0.015$, x_{Fe} or $x_{Co}=0.25\pm0.005$. Two $FePt_3$ samples hereafter labeled as $FePt_3$-*a* or -*b* having a slight difference in stoichiometry (iron excess of 2% in $FePt_3$-*a*) were prepared and studied.

After a homogenization anneal of some days at 1120 K the ingots were cut and shaped in the forms required for the further experiments, namely, powders for x-ray diffraction, thin foils for TEM and ordering kinetics experiments through resistivity measurements, and buttons for magnetic measurements. Then all the specimens were wrapped in Ta foils and sealed in evacuated silica tubes (10^{-4} Torr residual pressure) to undergo ordering thermal treatments. The temperatures and the times necessary to get the samples in the most ordered state of the $L1_2$ structure were deduced from the investigations of the ordering kinetics along the methodology developed by Dahmani *et al.*[4]

The basic principle for studying ordering kinetics by resistivity is as follows: a thin foil sample is mounted in an oven equipped for *in situ* automatized resistivity measurements. One performs a first anneal at a given temperature T below the order-disorder transition temperature until the equilibrium state corresponding to the equilibrium value of the long-range order (LRO) parameter η_T and characterized by a time invariant resistivity is attained. Then successive increasing and decreasing temperature steps were applied to the sample and the time variation of η through the measurement of resistivity was registered at each $T\pm\Delta T$ and fitted with the generally observed exponential behavior:

$$\frac{\Delta\rho^T(t)}{\Delta\rho^T_{\mathrm{eq}}(t=\infty)}=\int_0^\infty\left[1-\exp\left(\frac{-t}{\tau}\right)\right]P(\tau)d\tau. \qquad (1)$$

In relation (1) the probability $P(\tau)$ to observe the relaxation time τ is given by the lognormal distribution of width β:

$$P(\tau)=\frac{1}{\beta\sqrt{\pi}}\exp\left[-\left(\frac{\ln(\tau/\tau^T)}{\beta}\right)^2\right] \qquad (2)$$

and the other quantities represent $\Delta\rho^T(t)=\rho^T(t)-\rho^T(t=0)$ and $\Delta\rho^T_{\mathrm{eq}}(t=\infty)=\rho^T(t=\infty)-\rho^T(t=0)$.

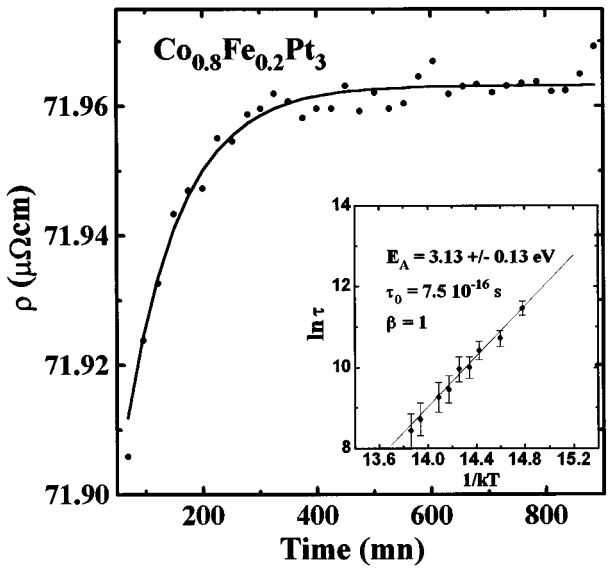

FIG. 1. An example of ordering kinetics in $Co_{0.8}Fe_{0.2}Pt_3$ set up by resistivity at 837.6 K (full circles) and fitted through relation (1) with $\beta=1$ (full line). In inset, Arrhenius plot of the average relaxation time τ^T set up with increasing and decreasing temperature steps, with its parameters.

An example of the kinetics set up in $Co_{0.8}Fe_{0.2}Pt_3$ is shown in Fig. 1. The temperature dependence of the center of gravity of the distribution τ^T is an Arrhenius law as illustrated in the inset of the figure. The parameters of the Arrhenius laws, i.e., τ_0, the preexponential factor, and E_A, the activation energy, allow us to calculate the time necessary to get the equilibrium state at any temperature, this time being considered as about $10\times\tau^T$. Comparing with the equivalent quantities determined by Dahmani *et al.*[4] in $CoPt_3$, a slight decrease of E_A with the Fe concentration is observed. This trend, as well as the important increase of the order-disorder transition temperature with increasing iron content (980 K in $CoPt_3$ and 1400 K in $FePt_3$) implies that the larger the Fe concentration, the greater the ability to develop the highest degree of order as well as the highest size of antiphase ordered domains.

At the end of the thermal treatment, Debye-Scherrer diffraction patterns set up on powders show all the lines of the $L1_2$ structure, yielding a precise determination of the lattice constant a as reported in Fig. 2. The $a(x)$ variation is represented by the line drawn through the experimental points taking into account an uncertainty of $\pm2\%$ on the stoichiometry as represented by the hatched area in the figure. The lattice constants present a monotonic variation with x, most of the experimental points displaying positive departures from Vegard's law. One composition ($x=0.7$) falls clearly below the uncertainty range, indicating an excess of 3*d* elements with respect to the stoichiometry that will have consequences on its magnetic properties.

TEM observations were performed on two compounds with $x=0.2$ and 0.4. Figure 3 shows a diffraction pattern near the [001] zone axis, revealing the strong intensities of the superstructure dots. Three dark field images formed by using, respectively, the superstructure diffracted beams $\vec{g}=$ [110], [210], and [120] reveal the presence of antiphase

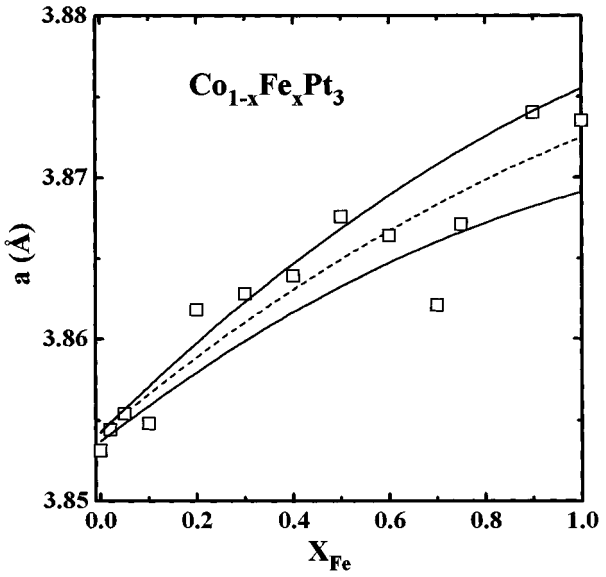

FIG. 2. Variation of the lattice constant a as a function of the Fe concentration. The dotted line is a fit of the experimental data. Solid lines represent the effect of $\pm 2\%$ composition uncertainties.

boundaries (APB's) and allow one to estimate the size of the ordered domains: between some tens and 100 nm.

As quantitative determinations of η are very time consuming, its maximum values attained at the end of the last ordering thermal treatment were estimated as in Ref. 2 from the theoretical curve calculated for the $L1_2$ structure using a cluster variation method.[4] The maximum values of η range between 0.97 on the Co-rich side and 1 on the Fe-rich side, as mainly resulting from the different values of T_{OD} in both compounds.

In conclusion, the total concentration of order defects in these alloys, including departures from stoichiometry, antisite defects, and atoms located at APB's, should not exceed a few percent. But these defects, when they correspond to excess of magnetic atoms with respect to stoichiometry, may have important effects on the magnetic properties, especially on the Fe-rich side.

III. MAGNETIC PROPERTIES

A. Brief overview of the 4 K magnetic behavior over the whole concentration range

After a rapid presentation of the experimental equipment, we present the main features of the magnetic phase diagram at low temperature deduced from the field dependence of the 4 K magnetization.

The experimental equipment used to investigate the magnetic properties over the whole concentration range are the same as those described in Ref. 2. We used several magnetometers working at various temperatures in magnetic fields ranging between low static fields (some mT) and pulsed high fields (35 T). A vibrating sample magnetometer (VSM), equipped with a variable temperature cryostat (4–300 K) and magnetic fields ranging up to 2 T, was used to determine the Curie temperatures and the field dependence of the magnetization in the low field range, and to detect the presence of irreversibilities on the magnetization curves. Let us mention that the occurrence of irreversibilities between the field cooled (FC) and the zero field cooled (ZFC) magnetization measured in low magnetic fields are the signature either of paramagnetic (P) to spin glass (SG) transitions or of ferromagnetic (F) or antiferromagnetic (AF) to reentrant spin-glass (RSG) transitions.[6] To complete low field measurements, high field magnetization was measured using two other magnetometers set up on identical basic principles, i.e., by integrating the flux variation induced by the sample submitted to the magnetic field in a pick-up coil. One of these magnetometers, equipped with a superconductor coil giving a maximum field of 4 T (SCM), works at 4 K. The high field experiments were performed at the Service National des Champs Magnétiques Pulsés (SNCMP) in Toulouse (France) in the slowly decreasing part of a pulsed field cycle (field rise time, 5 ms; field decay time, 500 ms) at 4 K up to 35 T. ac susceptibilities have also been measured in low alternating fields, but at a fixed frequency. As they did not bring complementary information with respect to the static susceptibilities, and as it is not the aim of the present contribution to study the dynamic response, such data are not presented here.

The field-dependent magnetization curves were set up at 4 K in the SCM equipment up to 4 T for all concentrations covering the whole concentration range from $x=0.02$ to 1. Figure 4 illustrates the three shapes of curves that correspond to three different magnetic states: those that display a clear ferromagnetic behavior on the Co-rich side ($x \leqslant 0.2$), the

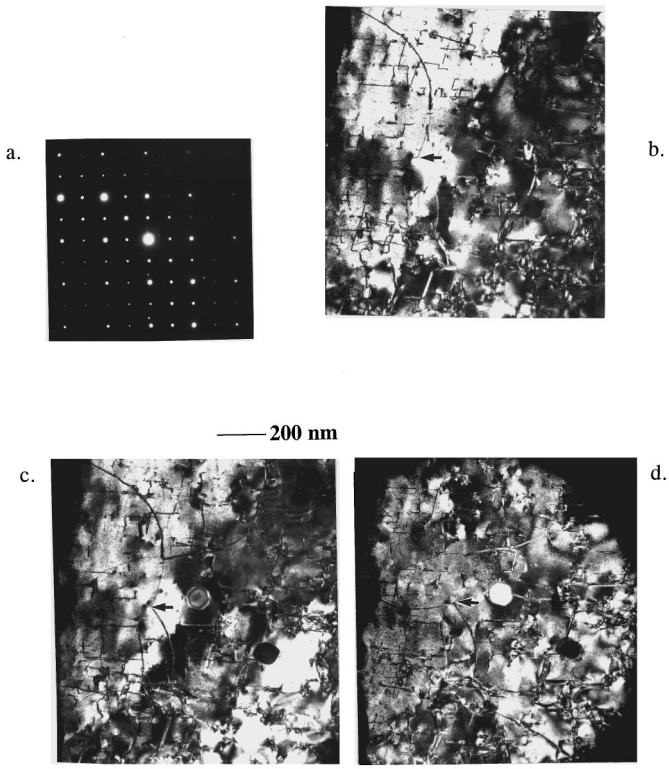

FIG. 3. (a) [001] zone axis diffraction patterns of $Co_{0.6}Fe_{0.4}Pt_3$ obtained in a 200 kV TOPCON transmission electron microscope (TEM) in two wave positions (000 and 011). (b), (c), and (d) Dark field images obtained with the three [110], [210], and [120] superstructure beams. The lines shown by the black arrows are the antiphase boundaries (APB's) as indicated by the fact that they are highlighted in two of the images and extinguished in the third one.

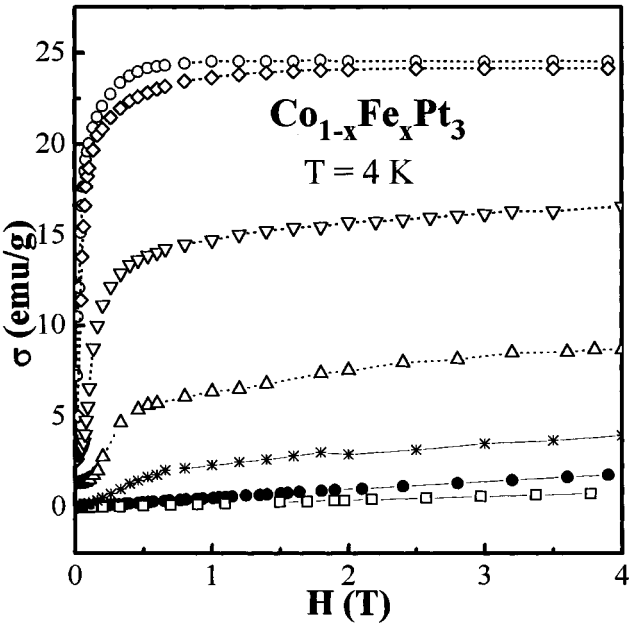

FIG. 4. 0–4 T field dependences of the 4 K magnetization set up in the SCM equipment. The curves correspond to $x=0.2$ (○), 0.3 (◇), 0.5 (∇), 0.6 (Δ), 0.75 (*), 0.8 (●), and 1 (□).

saturation being attained above 1 T, those that display an antiferromagnetic behavior on the Fe-rich side ($x>0.8$), and those in the intermediate concentration range ($0.2\leqslant x\leqslant 0.8$) that display a field-dependent initial susceptibility, the saturation not being reached in 4 T. In that intermediate range the low field part of the σ(H) curve displays a reentrant spin-glass (RSG) behavior characterized by an inverse curvature and an inflection point, which is generally observed in both F (Ref. 7) and AF RSG phases.[8] The field corresponding to this inflection point, which we call the threshold field ($H_{\rm thr}$), is plotted in Fig. 5 as a function of the concentration for all the investigated samples, except in the AF range

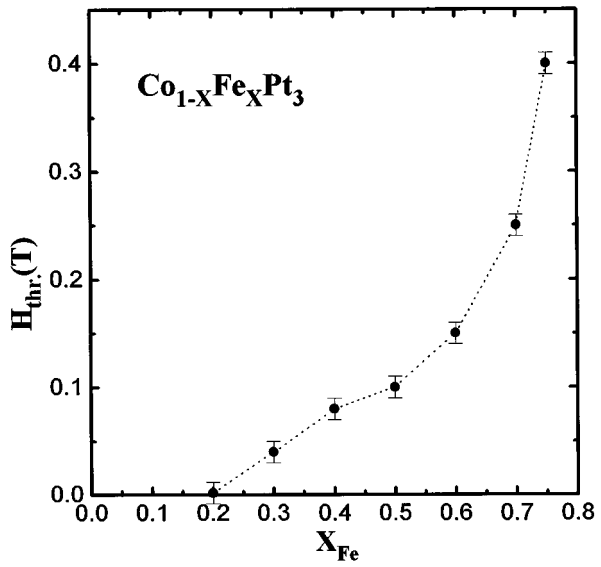

FIG. 5. Concentration dependence of the threshold field defined as the inflection point of the 4 K $\sigma(H)$ curves.

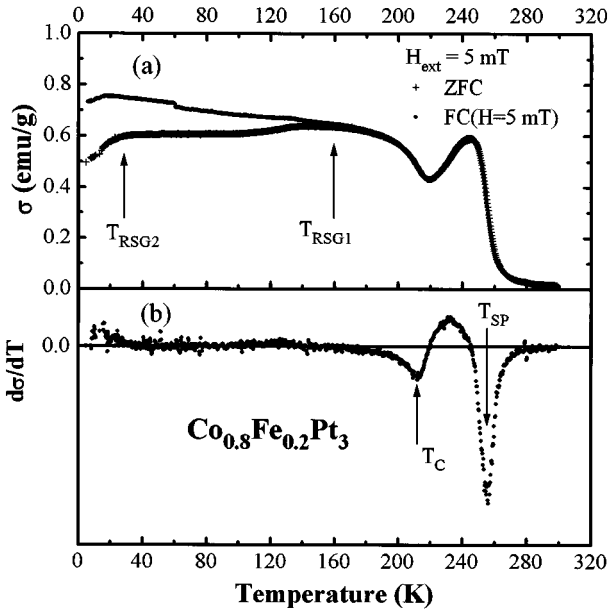

FIG. 6. Thermal variation of the magnetization and of its derivative measured in an applied field of 5 mT in $Co_{0.8}Fe_{0.2}Pt_3$. In (a) zero field cooled and field cooled magnetization curves are compared. The arrows indicate the positions of magnetic transitions as described in the text.

where it does not occur below 4 T. The threshold field occurs from around $x=0.2$ and increases with x, displaying an important change of slope between $x=0.5$ and 0.6. We shall show in the following sections that the concentration domain below $x=0.5$ corresponds to the occurrence of a reentrant spin-glass phase below a ferromagnetic phase, whereas above $x=0.5$ a mixed AF and spin-glass region occurs at low temperature until the occurrence of the pure antiferromagnetic region. This is the reason why the detailed results are presented in two different sections corresponding to iron concentrations below and above $x=0.5$.

B. Magnetic properties on the Co-rich side

First we present the low field properties that allow us to determine the low field phase diagram. Then we present the high field properties to get the saturation magnetization.

1. Limit of existence of a ferromagnetic order: Determination of Curie temperatures and of other magnetic transitions; Low field properties and low field phase diagram

The Curie temperatures were deduced from the thermal variation of the magnetization set up in the VSM in an external field of some mT. Most of the compounds display above T_C a superparamagnetic to paramagnetic transition ($T_{\rm SP}$). An example of the thermal variation of σ and of its temperature derivative $d\sigma/dT$ is shown in Fig. 6. The two temperatures T_C and $T_{\rm SP}$ are identified by the minima of the derivative curves as indicated by the arrows. The existence of a superparamagnetic state above T_C is evidenced from measurements performed in higher fields. As illustrated in Fig. 7 in $Co_{0.9}Fe_{0.1}Pt_3$ the superparamagnetic state disappears in an applied magnetic field of 0.1 T and the derivative

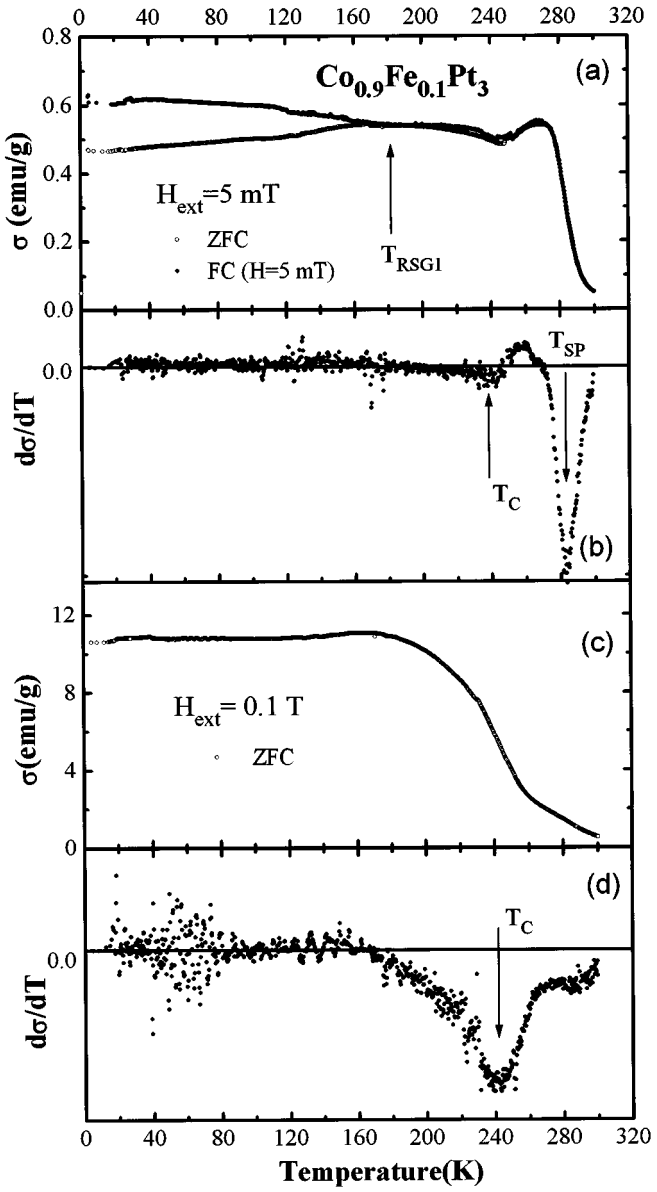

FIG. 7. (a) and (b) are the same as Figs. 6(a) and 6(b) measured in $Co_{0.9}Fe_{0.1}Pt_3$. T_{RSG1} denotes the first onset of irreversibilities. (c) and (d) show that the effect of a 0.1 T magnetic field is to suppress the superparamagnetic state.

[Fig. 7(d)] displays a single broad minimum around 240 K, corresponding to the Curie temperature. Both T_C and T_{SP} transitions are observed for $x=0.02$, 0.05, 0.1, 0.2, and 0.3. For $x=0.4$ and 0.5 the occurrence of a superparamagnetic state is not clearly evidenced. We have previously shown that, in the (Co-Mn)Pt_3 system,[2] the existence of superparamagnetism was correlated to the degree of LRO and to the size of ordered domains. In order to check whether the same correlation does exist also in these (Co-Fe)Pt_3 compounds, we submitted the $Co_{0.8}Fe_{0.2}Pt_3$ sample to an extremely long time anneal by multiplying by a factor of 10 the anneal times at each anneal temperature: the $\sigma(T)$ curve does not change at all, indicating that the presence of superparamagnetism is an intrinsic property of these compounds. The presence of superparamagnetism was also observed in Ref. 1 in the (Mn-Fe)Pt_3 system on the Mn-rich side.

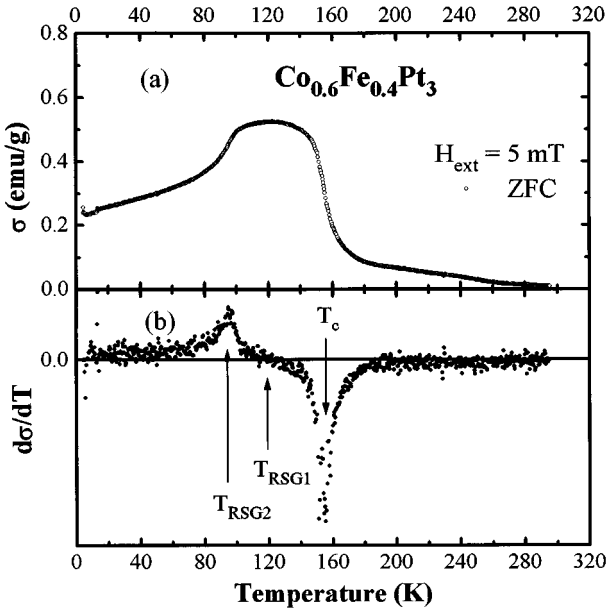

FIG. 8. Thermal variation of the ZFC magnetization and of its derivative measured in an applied field of 5 mT in $Co_{0.6}Fe_{0.4}Pt_3$.

Other striking characteristics of these ferromagnetic-like compounds are (i) the occurrence of irreversibilities between the zero field cooled (ZFC) and field cooled (FC) magnetization measurements (Figs. 6 and 7) and (ii) the existence of an inflection point on the low field part of the $\sigma(H)$ curves set up at 4 K (Fig. 4). Such behaviors are typical of the existence of reentrant spin-glass phases.[6,7]

Let us first consider the irreversibilities of $\sigma(T)$ at low fields. The first onset of irreversibility occurs for the lowest value of iron content (0.02) that we have investigated. This first and unique level of irreversibility is observed up to the iron content of 0.1. For $x=0.2$ and above, a second level of irreversibility characterized by a sharp decrease of the ZFC magnetization occurs at low temperature, as illustrated in Fig. 6. As these two irreversibility levels present the same features as those generally observed in reentrant spin-glass phases, we label them, respectively, T_{RSG1} and T_{RSG2}, in the same way as in the previous investigation of the (Co-Mn)Pt_3 system.[2,7] T_{RSG1} is identified as the maximum value of the ZFC $\sigma(T)$ curve, i.e., as the zero value of its derivative, and T_{RSG2} is identified by the sharp decrease on the ZFC curve, i.e., by the singularity on its derivative curve as indicated by the arrows in Figs. 7 and 8. Let us recall that these two reentrant spin-glass phases would correspond to the occurrence of the mixed phases (M_1 and M_2) described by Gabay and Toulouse,[9] the phase M_1 below T_{RSG1} being characterized by the coexistence of ferromagnetic order and a spin-glass ordering of the transverse component of the spins, and the phase M_2 below T_{RSG2}, which has the same coexistence of orderings as phase M_1 and has in addition the spontaneous breaking of the replica symmetry. The degree of frustration in phase M_2 is more important than in phase M_1, as it is closer to the spin-glass regime.

These two reentrant transitions were observed for $x=0.2$, 0.3, 0.4, and 0.5. When increasing x, both T_{RSG1} and T_C decrease, whereas T_{RSG2} increases, so that the three transitions tend to collapse at a certain concentration. Whereas as

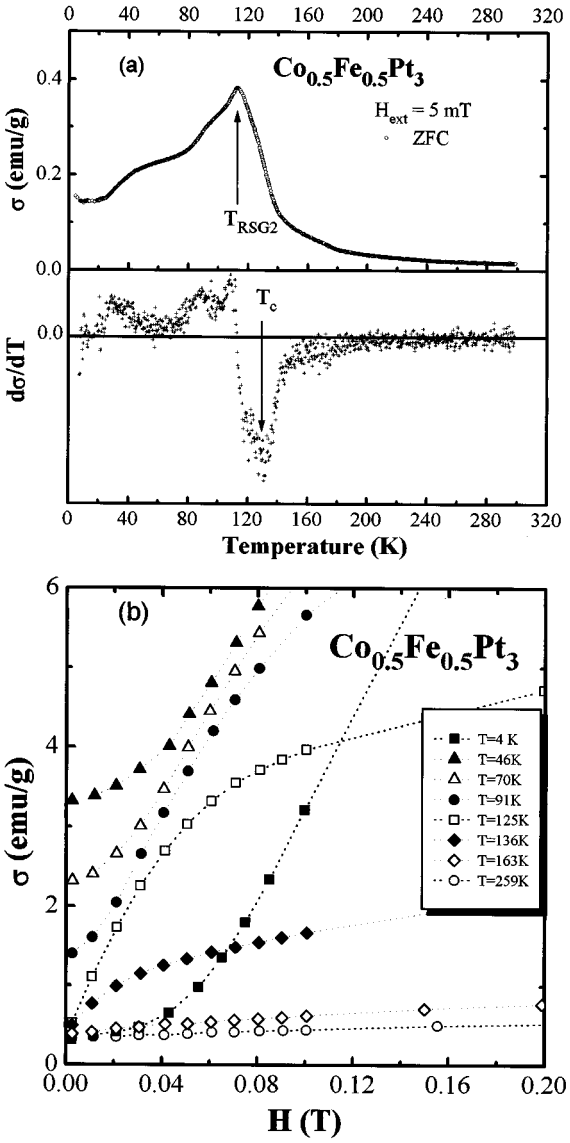

FIG. 9. (a) Thermal variation of the ZFC magnetization and of its derivative measured in an applied field of 5 mT in $Co_{0.5}Fe_{0.5}Pt_3$. (b) 0–0.2 T field dependences of the magnetization set up at various temperatures in $Co_{0.5}Fe_{0.5}Pt_3$.

shown in Fig. 8 for $x=0.4$ the three transitions are still well separated, for $x=0.5$ [Fig. 9(a)] it is difficult to separate T_{RSG1} and T_{RSG2} and both are close to T_C. The low field parts of $\sigma(H)$ set up at various temperatures in $Co_{0.5}Fe_{0.5}Pt_3$ are shown in Fig. 9(b). One observes the disappearance of the reentrant spin-glass-like behavior between 91 K and 125 K. At 125 K the field dependence is that of a ferromagnetic compound, whose Curie temperature is located between 136 K and 163 K, as revealed by the paramagnetic behavior above 163 K. This composition is an interesting one as it represents the highest iron concentration of the series, scanned with a 0.1 concentration step, that displays a ferromagnetic behavior on a certain temperature range. These results are in qualitative agreement with those shown on Fig. 9(a) that locate T_C at 130 ± 10 K.

As already shown in Figs. 4 and 5, a field-dependent initial susceptibility is observed for $x>0.1$ until a threshold

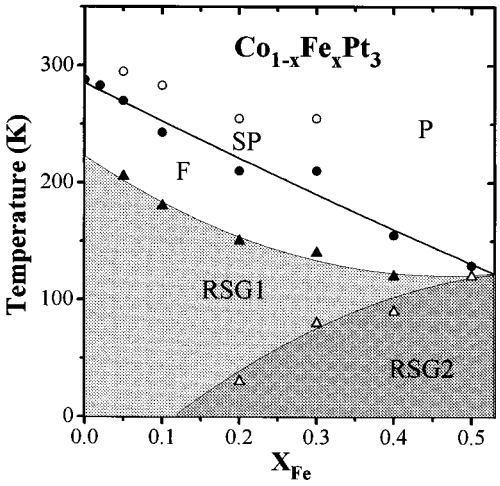

FIG. 10. Tentative low field phase diagram of the Co-rich side, showing the existence ranges of the paramagnetic (P), ferromagnetic (F), and reentrant spin-glass (RSG1 and RSG2) phases and the occurrence of a multicritical point around $x=0.55$ and $T=120$ K.

field (H_{thr}), which increases rapidly with x above $x=0.2$. This concentration corresponds also to the occurrence of the strong level of irreversibility T_{RSG2}.

To summarize the results obtained on the Co-rich side, we have reported on Fig. 10 the temperatures of all the identified magnetic transitions observed for $x<0.6$. It seems clear that the lines $T_C(x)$, $T_{RSG1}(x)$, and $T_{RSG2}(x)$ converge towards a multicritical point which could be located around $x=0.55$ and $T\approx120$ K. Above this concentration a long-range ferromagnetic order does not appear anymore, and as shown in Sec. III C, the magnetic ordering is either a pure spin-glass ordering or a mixed spin-glass and antiferromagnetic ordering. Assuming that the ferromagnetic region is closed by a vertical critical line, we delimit on this Co-rich side below the paramagnetic (or superparamagnetic) to ferromagnetic transition three regions corresponding to three magnetic states: ferromagnetic (region F), reentrant spin-glass phase of type 1 (region RSG1), and reentrant phase of type 2 (region RSG2), as indicated on the figure. The phase diagram will be discussed in Sec. IV.

2. High field behavior: Saturation magnetizations

More information on these mixed phases can also be obtained from the high field behavior. On the Co-rich side ($0.02\leqslant x\leqslant0.2$), the magnetization measured in the SCM equipment displays a saturation above 1 T. The values of the saturation magnetization deduced from a zero field extrapolation ($\sigma_{s,H=0}$) are plotted in Fig. 11 as a function of x. For comparison, above $x=0.2$, the values of σ in the maximum field of 4 T are also shown. A linear dependence of $\sigma_{s,H=0}$ on x is observed below 0.2, whose extrapolation to $x=1$ yields an average magnetic moment of $0.88\mu_B$ in $FePt_3$. This value corresponds to a moment of $2.9\mu_B$ on the Fe atoms, assuming a moment of $0.2\mu_B$ on the Pt atoms, a result which is in qualitative agreement with neutron diffraction data reported by Bacon and Crangle.[3] The linear behavior of $\sigma_{s,H=0}$ with x for $x\leqslant0.2$ would mean that (i) a magnetic

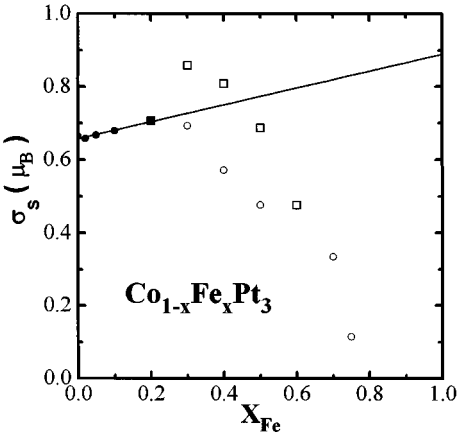

FIG. 11. Concentration dependence of the 4 K magnetization. The dark circles represent the saturation values, and the open circles are the values of the magnetization in a field of 4 T obtained with the SCM equipment. The open squares are the values extrapolated towards an infinite field deduced from the high field measurements at the SNCMP, and normalized to the saturation value at $x=0.2$ as measured with the SCM equipment. For $x=0.7$, the 4 K magnetization is higher than expected from an extrapolation between 0.5 and 0.75. This can be explained by an excess of 3*d* metal as shown by its lattice parameter value (Fig. 2).

field of 1 T is sufficient to align all the magnetic moments along the applied field, and (ii) on average the Co and Fe moments are concentration independent. Above $x=0.2$ the magnetization values in a field of 4 T depart strongly from the linear behavior and decrease rapidly with x.

The 4 K magnetization curves set up at the SNCMP of Toulouse up to 35 T are shown in Fig. 12. For $x=0.3$, 0.4, and 0.5 one observes a continuous increase of the magnetization with the field without saturation being achieved in the highest field of 35 T. Such a behavior is that of a reentrant spin-glass phase, being the signature of randomly canted spin states as previously observed in the $Co_{1-x}Mn_xPt_3$ system for $0<x\leqslant 0.8$,[2] or in the canonical Au-Fe spin glasses.[10,11] For $x=0.6$ the shape of the $\sigma(H)$ curve is different, showing around 6–7 T a field transition that could be a spin-flip transition. As previously mentioned, this composition falls out of the concentration range where a ferromagnetic order coexists with a spin-glass order. Its properties will be discussed in the following section. Trying to get the 4 K saturation values, we extrapolated the high field data towards infinite field by plotting σ against $1/H$. The results are shown as squares on Fig. 11. For $x=0.3$ and 0.4 the extrapolated values are superior to the $\sigma(x)$ linear behavior observed in low fields (straight line of Fig. 11) as if an infinite field aligns all the magnetic moments along the applied field, even yielding an extra magnetic contribution. The same kind of behavior was also observed in the (Co-Mn)Pt_3 system.[2] For $x=0.5$, the extrapolated value departs slightly from the $\sigma(x)$ linear behavior, indicating that the saturation limit is not totally attained (probably due to the presence of some AF clusters). For $x=0.6$, the departure from saturation is higher, but this composition belongs to a different region of the phase diagram, discussed in the following section.

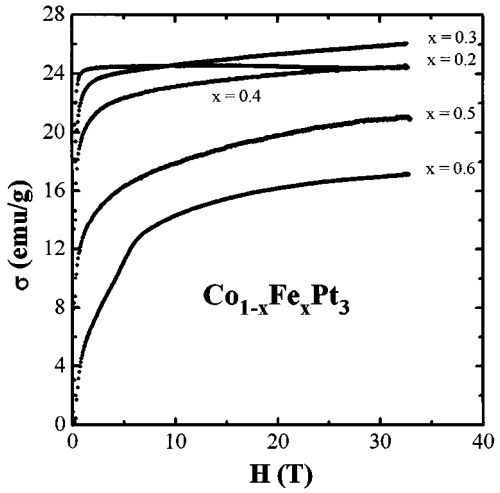

FIG. 12. 0–35 T field dependences of the 4 K magnetization set up at the SNCMP of Toulouse for different concentrations.

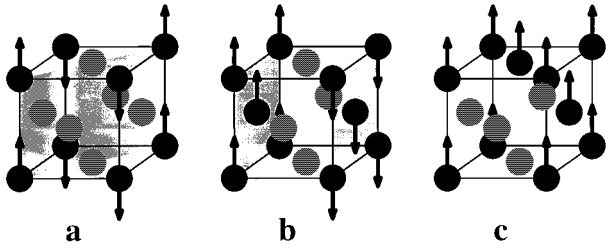

FIG. 13. Magnetic and structural arrangements in $FePt_3$ giving rise to (a) antiferromagnetic $[\frac{1}{2}\frac{1}{2}0]$, (b) antiferromagnetic $[\frac{1}{2}00]$, and (c) ferromagnetic [100] reflections [from Bacon and Crangle (Ref. 3)].

C. Magnetic properties on the Fe-rich side

The magnetic properties of the $Co_{1-x}Fe_xPt_3$ compounds on the iron-rich side ($x\geqslant 0.6$) were investigated by using the same equipment as in Sec. III B. It is clear, as we shall see, that for compounds which display competing antiferromagnetic and spin-glass orders, the measurement of macroscopic properties is not sufficient to get a precise insight into the magnetic orders. Neutron diffraction measurements should be performed. The results we present in this section have thus to be considered as preliminary ones.

In a first section, we present and discuss the properties of $FePt_3$ around the stoichiometric composition. First we recall the main features of its antiferromagnetic structure as investigated by neutron diffraction by Bacon and Crangle[3] and by Mössbauer spectroscopy by Palaith *et al.*[12] Then we present our susceptibility data. The following section will be devoted to the magnetic properties of ternary compounds having between 0.6 and 0.9 iron atomic fraction.

1. $FePt_3$

Previous studies. The magnetic structural arrangements of $FePt_3$ as investigated by Bacon and Crangle[3] for iron compositions between 24% and 36% are drawn in Fig. 13. At the $FePt_3$ stoichiometry the coupling of the iron moments gives rise to (110) ferromagnetic sheets with adjacent sheets arranged antiferromagnetically. This ordering produces the

$[\frac{1}{2}\frac{1}{2}0]$ spin modulation [Fig. 13(a)]. When iron atoms are added to the system, they begin to occupy the face-center sites; nearest-neighbor (NN) iron atoms couple into (100) ferromagnetic sheets which in turn couple with each other antiferromagnetically to give the $[\frac{1}{2}00]$ order [Fig. 13(b)]. With further increase of the iron concentration, increasing numbers of iron atoms go into face centers and ferromagnetic ordering results as shown in Fig. 13(c). The order in all cases is long range. The iron moment was found to be $\approx(3.3\pm0.3)\mu_B$ for both antiferromagnetic structures and $\approx2\mu_B$ for the ferromagnetic one. The moment of platinum is less than $0.2\mu_B$ for all compositions. At the stoichiometry, the Néel temperatures of the $[\frac{1}{2}\frac{1}{2}0]$ and $[\frac{1}{2}00]$ structures are, respectively, 160 K and 100 K. The $[\frac{1}{2}00]$ structure is stabilized with increasing iron content and its Néel temperature increases until 130 K for 28 at. % Fe and saturates above this composition, whereas the Néel temperature of the $[\frac{1}{2}\frac{1}{2}0]$ structure decreases slightly with increasing iron content and the $[\frac{1}{2}\frac{1}{2}0]$ order is not present in the alloy with 28 at. % Fe. Let us note that in the $[\frac{1}{2}\frac{1}{2}0]$ structure, four of the Fe-Fe *NN* interactions are AF and two are *F*, i.e., are frustrated bonds, whereas in the $[\frac{1}{2}00]$ structure, there are only two AF interactions and four frustrated bonds. In terms of frustrations, the $[\frac{1}{2}00]$ structure is more frustrated than the $[\frac{1}{2}\frac{1}{2}0]$ structure. Surprisingly, the $[\frac{1}{2}\frac{1}{2}\frac{1}{2}]$ structure which would not be frustrated is not observed.

To summarize, the basic magnetic structure of stoichiometric and ordered $FePt_3$ is the $[\frac{1}{2}\frac{1}{2}0]$ AF order, but, even for the stoichiometric composition, the atomic disordering and the presence of APB's introduce either the $[\frac{1}{2}00]$ AF order or ferromagnetism by creating nearest-neighbor iron arrangements.[13,14] It seems clear also that, even in the presence of frustrated bonds and even of some atom disorder, a collinear order along the [100] direction is preferred to some canted or random spin state.

Our data. The field dependence of the 4 K magnetization is shown in Fig. 14(a) for the two prepared $FePt_3$-*a* and $FePt_3$-*b* compounds. $FePt_3$-*b* displays a linear $\sigma(H)$ curve as expected for a pure antiferromagnetic phase, whereas the $\sigma(H)$ curve of $FePt_3$-*a* presents a small curvature at low field that could be assigned to the presence of some ferromagnetic clusters. Such a behavior is not surprising for this compound, which has been prepared with a small iron excess with respect to stoichiometry. If the iron atoms in excess occupy the centers of the faces, a ferromagnetic behavior is expected [Fig. 13(c)]. Thus in the following we discard the study of $FePt_3$-*a*. This point also emphazises the important role played by the stoichiometry defects in the ternary AF phases when the departure from stoichiometry arises from an excess of Co or Fe atoms.

The temperature dependence of the inverse susceptibility $(1/\chi)$ of $FePt_3$-*b* measured in a field of 2 T is plotted in Fig. 14(b). The curve displays two singularities: a sharp minimum is observed around 80–90 K, and $1/\chi$ departs from a *T*-linear behavior at 160 K. In the following, we assign these two singularities, T_{N1} and T_{N2}, respectively, to the Néel temperatures of the $[\frac{1}{2}\frac{1}{2}0]$ and $[\frac{1}{2}00]$ antiferromagnetic structures, as identified in Ref. 3. Let us recall that the $[\frac{1}{2}\frac{1}{2}0]$ structure corresponding to the highest Néel temperature of 160 K is the basic antiferromagnetic order which should be

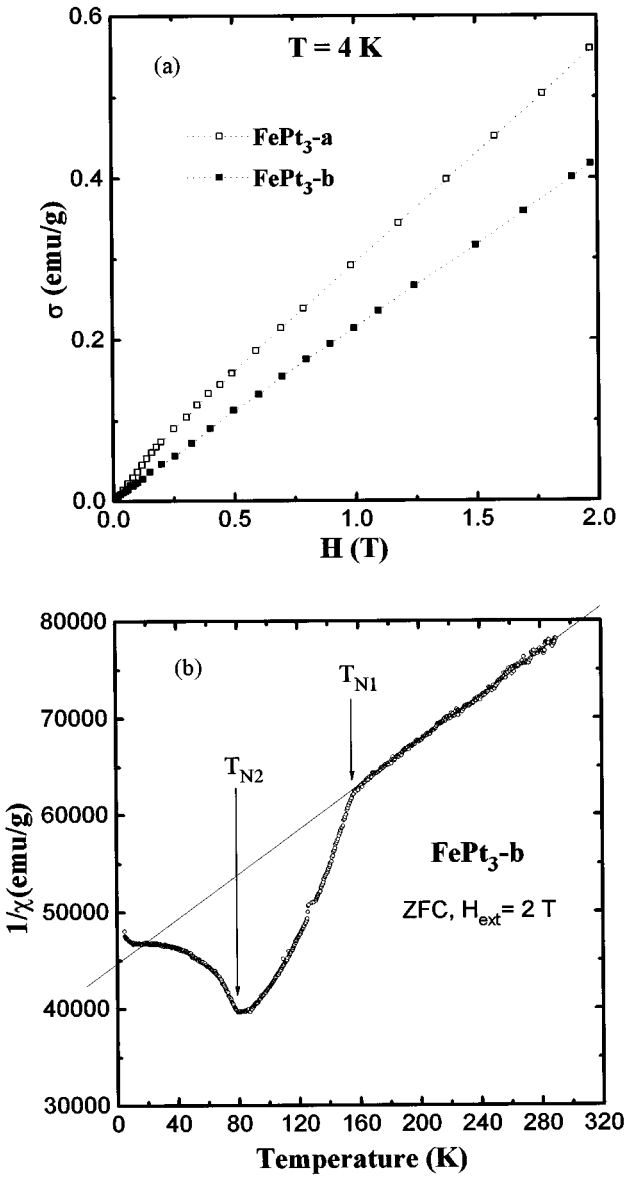

FIG. 14. (a) Field dependence of the 4 K magnetization in $FePt_3$-*a* and $FePt_3$-*b*. (b) Inverse susceptibility versus temperature in $FePt_3$-*b* measured in a field of 2 T.

observed in the stoichiometric $FePt_3$ compound. From the Curie-Weiss law observed above 160 K, one deduces from the Curie constant an effective number of moment carriers (n_{eff}) of $2.52\mu_B$. This value is high compared to the value of $0.88\mu_B$ obtained by extrapolation in Fig. 11, giving a ratio of 2.9 between both values, which is in favor of an itinerant magnetism in these compounds, a ratio of 1 being expected in systems with localized magnetic moments.[15]

2. Ternary $Co_{1-x}Fe_xPt_3$ compounds for $0.6\leqslant x<1$

The 4 K field dependences of the magnetization shown in Fig. 4 display a clear change of behavior between 0.8 and 0.75 from a pure antiferromagnet [linear $\sigma(H)$] to a mixed spin-glass antiferromagnet (**S**-shaped curve).

If the 4 K $\sigma(T)$ curves are similar for $x=0.9$ and 0.8, the *T* dependences of their susceptibility in various magnetic fields are different. Figure 15 compares the $1/\chi(T)$ curves set up in a field of 2 T in $Co_{0.1}Fe_{0.9}Pt_3$ and in fields of 0.02 and

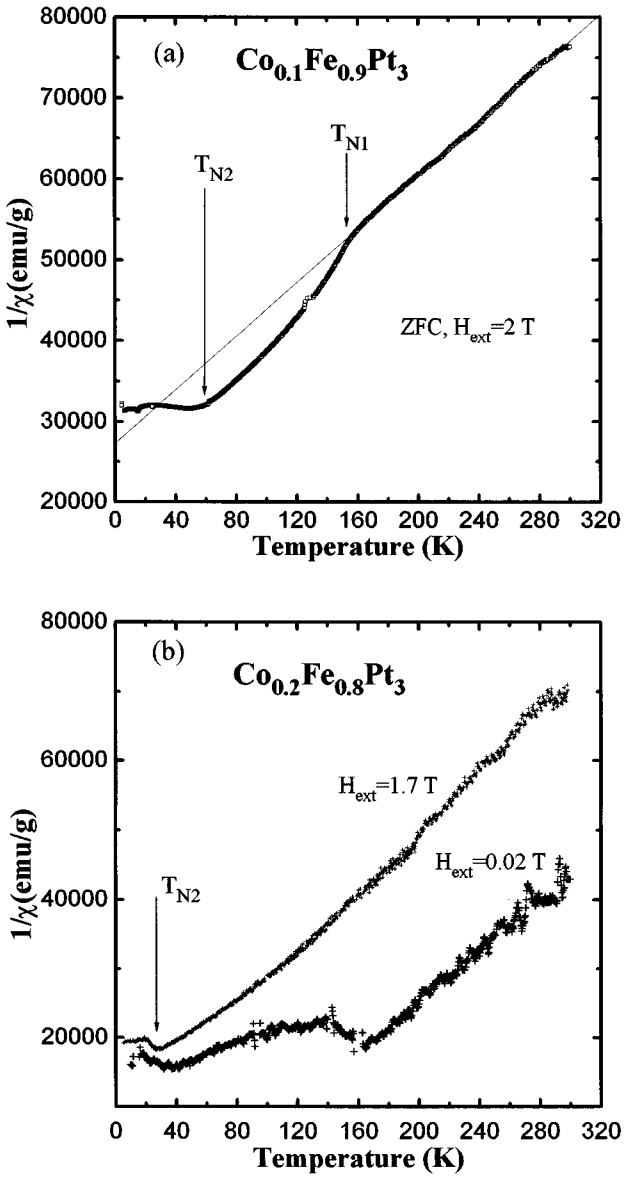

FIG. 15. Inverse susceptibility versus temperature in $Co_{0.1}Fe_{0.9}Pt_3$ measured in a field of 2 T (a) and in $Co_{0.2}Fe_{0.8}Pt_3$, measured in fields of 0.02 and 1.7 T (b).

1.7 T in $Co_{0.2}Fe_{0.8}Pt_3$. For $x=0.9$ the two Néel temperatures are observed at, respectively, 160 K and 60 K in a field of 2 T. For $x=0.8$ both Néel temperatures are observed in the smaller field of 0.02 T at, respectively, 160 K and around 30–40 K, whereas in the field of 1.7 T the transition at 160 K has disappeared but T_{N2} is still observed at 30 K. The disappearance of T_{N1} with increasing magnetic field is also observed in other compounds with $x=0.75$ (Fig. 16) and $x=0.7$ (Fig. 17). For $x=0.75$, T_{N1} disappears between 0.1 and 0.2 T, without observing an appreciable shift with the applied field. For $x=0.7$, we clearly observe the decrease of T_{N1} with increasing H until it is indistinguishable from T_{N2} in a field of 1 T. All these features, showing the extreme sensitivity of T_{N1} to the magnetic field for $0.6 \leqslant x \leqslant 0.8$, are the signature of a spin-glass to paramagnetic transition (see, for example, Lefloch *et al.*[16] and references therein). This indicates that the $[\frac{1}{2}\frac{1}{2}0]$ antiferromagnetic-paramagnetic transition changes progressively into a spin-glass–paramagnetic transition when increasing the Co content. Confirmation of the presence of a spin-glass-like phase below T_{N1} from $x \leqslant 0.8$ is shown by the existence of strong irreversibilities between the ZFC and FC magnetization curves as illustrated in Fig. 18 for $x=0.8$, 0.75, and 0.7 and by ac susceptibility measurements. For example, for $x=0.7$ both components χ' and χ'' of the ac susceptibility set up in 2×10^{-2} mT and 80 Hz display a sharp maximum at 160 K. This temperature is slightly higher than the spin-glass–paramagnetic transition measured in 5 mT, but it is in agreement with the value expected from the field dependence of T_{SG} (see Fig. 17). The lower Néel temperatures T_{N2} are not visible after cooling in a magnetic field. Without more detailed measurements such as neutron diffraction, it is difficult to identify the nature of this transition in the 0.6–0.8 concentration range. As this transition is not a fundamental transition of $FePt_3$ and *a fortiori* of the ternary phase diagram, we did not further explore this point.

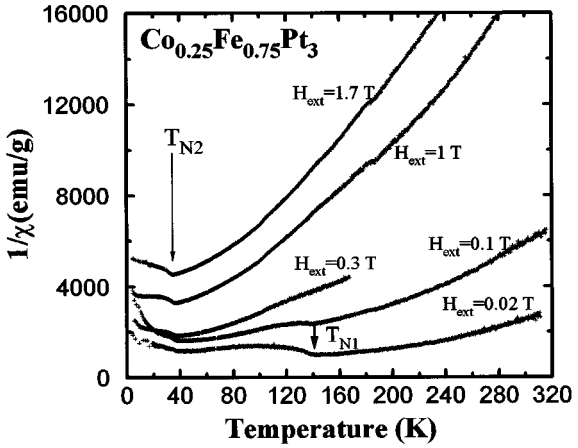

FIG. 16. Temperature dependence of $1/\chi$ in $Co_{0.25}Fe_{0.75}Pt_3$ at various fields.

Being aware of the complexity of the magnetic orders in $FePt_3$ and in ternary phases, the tentative iron-rich phase diagram we propose is drawn in Fig. 19(a) together with the Co-rich side drawn in Fig. 10. It seems clear that, in addition to a narrow pure AF region spreading from $FePt_3$ to $Co_{0.2}Fe_{0.8}Pt_3$, there is a spin-glass region between 0.6 and 0.8 over a relatively broad T range which coexists with the $[\frac{1}{2}00]$ AF or AF-SG order below 40 K. The spin-glass region seems to be the continuation of the RSG phase (RSG2) observed on the ferromagnetic side below 0.55. We did not observe a RSG phase on the AF side.

IV. DISCUSSION

The total (Co-Fe)Pt_3 phase diagram resulting from this study is compared in Fig. 19 with the experimental (Mn-Fe)Pt_3 and (Co-Mn)Pt_3 phase diagrams previously determined.

In the (Co-Fe)Pt_3 system, the occurrence of a spin-glass region separating the ferromagnetic and antiferromagnetic regions of an $A_{1-x}B_x$ system, where A and B are, respectively, a ferromagnet and an antiferromagnet, is predicted by many theoretical models, but has been rarely observed ex-

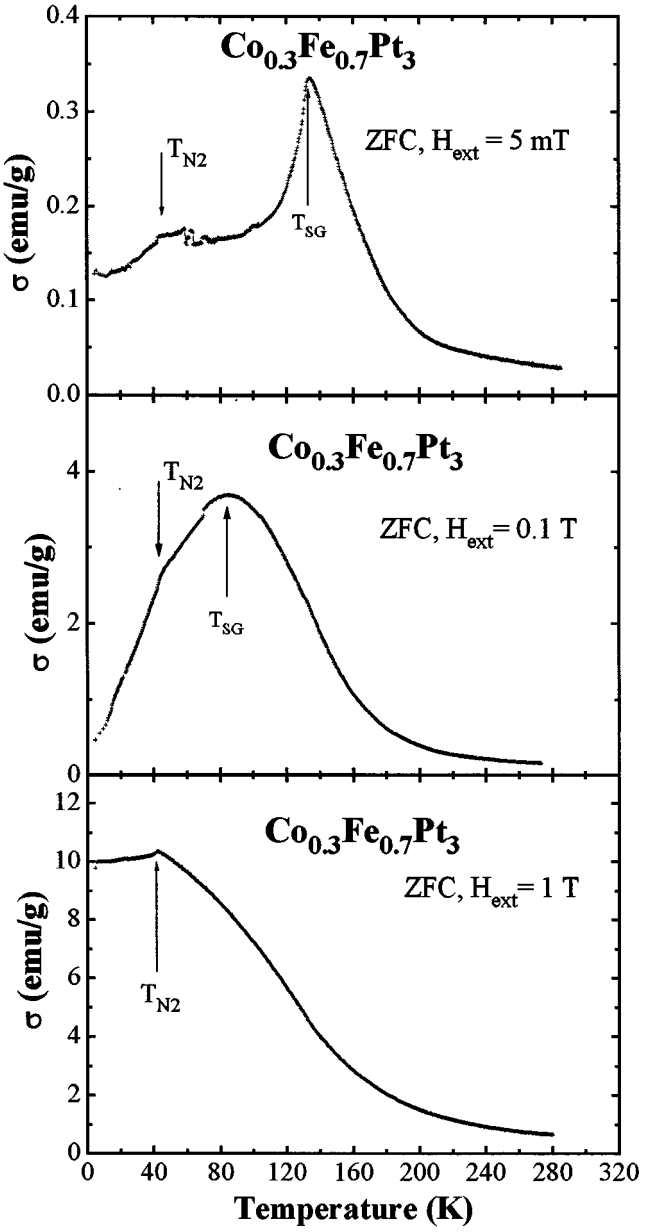

FIG. 17. Effect of the applied magnetic field on the ZFC magnetization curve in $Co_{0.3}Fe_{0.7}Pt_3$.

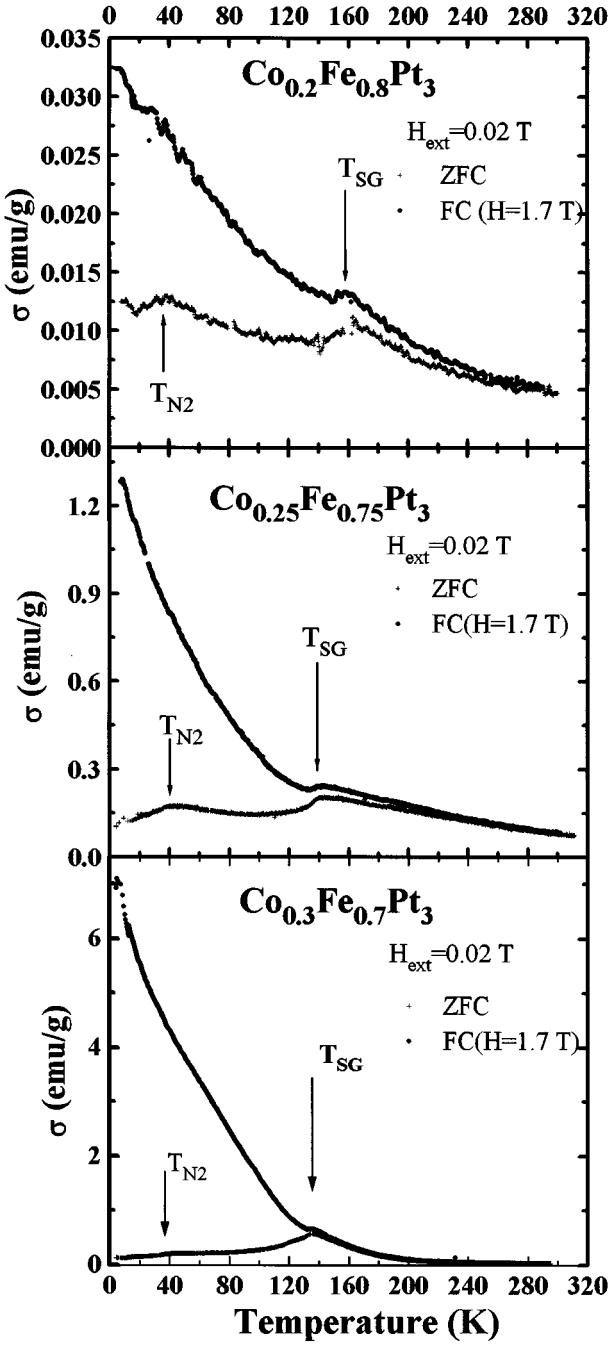

FIG. 18. Irreversibilities between the ZFC and FC (1.7 T) magnetization curves set up in a field of 0.02 T in $Co_{0.2}Fe_{0.8}Pt_3$, $Co_{0.25}Fe_{0.75}Pt_3$, and $Co_{0.3}Fe_{0.7}Pt_3$.

perimentally (see, for example, the $Eu_{1-x}Gd_xS$ system[17]). Most of the experimental metallic systems do not cover the total concentration range for structural phase stability reasons, such as, for example, the well-known Ni-Mn, Au-Fe, or Fe-Mn systems. Many theoretical approaches have been developed to describe the magnetic phase diagrams of systems with competing magnetic interactions for both Ising and Heisenberg spins. In order to describe the occurrence of spin-glass and reentrant spin-glass phases below ferromagnetic or antiferromagnetic order in systems presenting competing magnetic interactions, one can say that, on the whole, the theoretical models separate into two main classes: the homogeneous models such as, for example, the Gabay-Toulouse (GT) picture,[9] and inhomogeneous pictures.[18–20] In the GT model, the coexistence of long-range ferromagnetic (or antiferromagnetic) order and spin-glass order takes place simultaneously everywhere in the material. In inhomogeneous pictures, the system is divided into two regions or networks, one network where ferromagnetic (or antiferromagnetic) interactions are strong and another network where random interactions giving rise to the SG order dominate. But both approaches give rise to similar phase diagrams characterized by the occurrence of a spin-glass region that separates the ferromagnetic and antiferromagnetic sides as observed in the $(Co\text{-}Fe)Pt_3$ phase diagram. More recently a three-dimensional (3D) site-random Heisenberg model[20] of ferromagnetic and antiferromagnetic ions predicts, in an in-

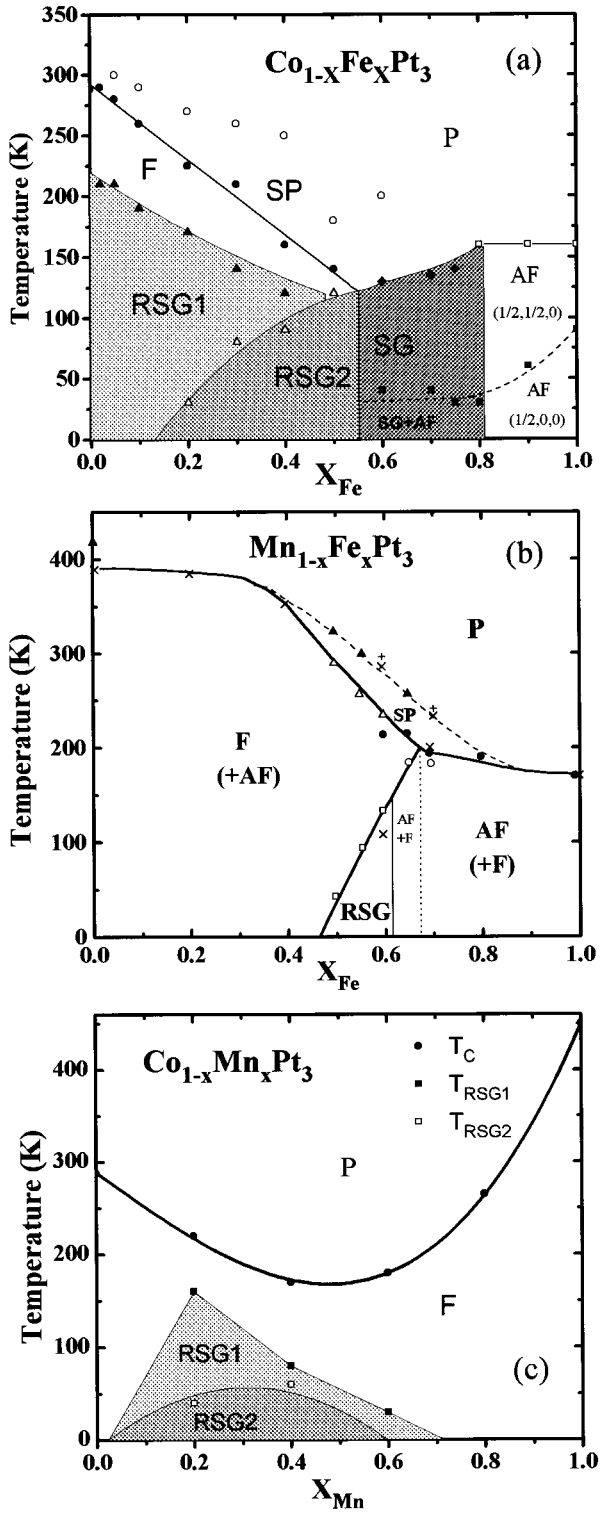

FIG. 19. Tentative (Co-Fe)Pt_3 magnetic phase diagram as deduced from the present investigation (a) compared with the (Fe-Mn)Pt_3 phase diagram from Ref. 1 (b) and with our previous determination (Ref. 2) of the (Co-Mn)Pt_3 phase diagram (c).

termediate concentration range, the occurrence of a mixed phase of longitudinal ferromagnetism and transverse antiferromagnetism with two decoupled order parameters, which would be rather relevant for the (Mn-Fe)Pt_3 phase diagram.

Without more detailed investigations, it is difficult *a priori* to say whether the (Co-Fe)Pt_3 system is relevant for homogeneous or inhomogeneous models. In our previous investigation of the (Co-Mn)Pt_3 system, we found that its phase diagram matches fairly well the GT model, i.e., it can be treated as a homogeneous system. In this system, which is a rare example of the occurrence of RSG phases when alloying two ferromagnetic compounds, the random mean exchange field was shown to arise from the negative sign of the mixed Co-Mn interaction in simulations of the phase diagram by using the approach developed by Basu and Ghatak[21] for Ising spins on a disordered lattice.[22] The case of (Co-Fe)Pt_3 seems to be somewhat different. The weakly frustrated RSG1 phase occurs at Fe concentration as low as 2% (Fig. 10) which corresponds to a very small concentration of frustrated bonds insufficient to induce a random exchange field throughout the whole material. It is clear that the occurrence of irreversiblities at such low iron concentrations would be in favor of a negative Co-Fe interaction, since in that case, each iron atom introduces six frustrated bonds, and 2% of iron atoms with respect to Co atoms represent 12% of frustrated bonds. This is enough to build a network (or clusters) of frustrated bonds but not to induce a homogeneous random exchange field throughout the sample. If J_{CoFe} is positive, one does not expect the occurrence of a frustrated phase before an appreciable concentration of NN AF Fe-Fe pairs, i.e., at Fe concentrations clearly higher than 2%, in disagreement with the phase diagram. Below $x=0.2$, i.e., before the occurrence of the RSG2 phase, the magnetic state of the system would be inhomogeneous, the percolated ferromagnetic regions being separated by either a network or clusters of randomly canted spins. Between $x=0.2$ and 0.55, the experimental phase diagram matches the GT schematic phase diagram, as the (Co-Mn)Pt_3 does. That means that the succession of phases encountered at various temperatures is the same in both phase diagrams, considering that the experimental Curie temperatures are an indication of the average exchange interaction (J) of the GT model. Thus on the ferromagnetic side of the (Co-Fe)Pt_3 phase diagram, one would pass progressively at low temperature and low magnetic field from a mixed inhomogeneous magnetic state to a homogeneous randomly canted spin state around $x=0.2$.

On the iron-rich side, the stability of the AF structures with increasing Co content up to 0.2 is also consistent with a negative value of J_{CoFe} as a negative sign of J_{CoFe} is expected to have little influence on the AF structures. Only the occurrence of an appreciable concentration of NN F Co-Co interactions will destroy the AF order, as observed by the occurrence of the spin-glass behavior around $x=0.8$.

Comparing the (Co-Fe)Pt_3 ternary phase diagram with the (Mn-Fe)Pt_3 one, whose terminal phases have the same magnetic properties, they are relatively different. Whereas a point in common is the nonappearance of RSG phases on the AF side, they have two main differences: (i) a spin-glass region separates the ferromagnetic side from the antiferromagnetic one in (Co-Fe)Pt_3 and not in (Mn-Fe)Pt_3; (ii) two broad reentrant spin-glass regions occur on the ferromagnetic side of (Co-Fe)Pt_3 starting at very low iron content, whereas a single narrow RSG phase is observed in (Mn-Fe)Pt_3 from

iron content as high as about 0.5. Let us also mention that the two kinds of antiferromagnetic order are not set up on the AF side of (Mn-Fe)Pt_3.

From this comparison we deduce that the (Co-Fe)Pt_3 system must be more frustrated than the (Mn-Fe)Pt_3 one. The weakness of the ferromagnetic Co-Co interaction with respect to the Mn-Mn interaction [$T_C(CoPt_3)/T_C(MnPt_3) = 0.64$],[2] could be one of the reasons for this. Another cause might be the sign and strength of the mixed Co-Fe and Mn-Fe interactions. The nonoccurrence of both a RSG phase before $x \approx 0.5$ and a pure SG phase at the intermediate concentration range is in favor of a positive Fe-Mn interaction, as also claimed by Schreiner *et al.*[1] But one can also suggest that the collinear F or AF orders are more stable than canted spin states in the (Mn-Fe)Pt_3 system, as described in Ref. 20.

To conclude, we have now on hand the three ternary magnetic phase diagrams built from the $CoPt_3$ and $MnPt_3$ ferromagnets and the $FePt_3$ antiferromagnet, which display relatively different magnetic behaviors, emphasizing the important role played by the sign and the strength of the mixed interaction. Further experiments such as neutron depolarization and magnetic neutron diffraction are still planned to study the spatial fluctuations of the magnetization density on a mesoscopic scale in reentrant spin-glass phases and to determine the different magnetic orders in the compounds that display antiferromagnetism. In any case, even if these compounds do not really belong to the family of localized spin systems, we think that their phase diagrams can serve as models for testing theoretical approaches, based on Heisenberg or Ising spins, treated at various levels of point, pair, or larger cluster approximations. Until now the cluster variation method (CVM), currently used to reproduce chemical phase diagrams, was rarely applied to magnetic phase diagrams.

---

*Present address: Department of Physics, POSTECH, San 31 Hyoja-dong Pohang 790-784, Republic of Korea.

[1] W.H. Schreiner, W. Stamm, and E.F. Wassermann, J. Phys. F **15**, 2009 (1985).
[2] T.H. Kim, M.C. Cadeville, A. Dinia, and H. Rakoto, Phys. Rev. B **53**, 221 (1996).
[3] G.E. Bacon and J. Crangle, Proc. R. Soc. London Ser. A **272**, 387 (1963).
[4] C.E. Dahmani, M.C. Cadeville, and V. Pierron-Bohnes, Acta Metall. **38**, 2199 (1985).
[5] M.C. Cadeville, V. Pierron-Bohnes, L. Bouzidi, and J.M. Sanchez, Phys. Scr. **T49**, 364 (1993).
[6] Ch. Böttger, R. Stasch, A. Wulfes, and J. Hesse, J. Magn. Magn. Mater. **99**, 280 (1991).
[7] T.H. Kim, Ph.D. thesis, Louis Pasteur University, Strasbourg, France, 1994.
[8] H. Aruga Katori, T. Goto, S. Ebii, and A. Ito, J. Magn. Magn. Mater. **104**–**107**, 1639 (1992).
[9] M. Gabay and G. Toulouse, Phys. Rev. Lett. **47**, 201 (1981).
[10] H. Rakoto, J.C. Ousset, S. Senoussi, and I.A. Campbell, J. Magn. Magn. Mater. **46**, 212 (1984).
[11] I.A. Campbell and S. Senoussi, Philos. Mag. B **65**, 1267 (1992).
[12] D. Palaith, C.W. Kimball, R.S. Preston, and J. Crangle, Phys. Rev. **178**, 795 (1969).
[13] S. Takahashi and K. Ikeda, Phys. Rev. B **28**, 5225 (1983).
[14] S. Takahashi and A.Y. Takahashi, J. Phys. Condens. Matter **4**, L339 (1992).
[15] P.R. Rhodes and E.P. Wohlfarth, Proc. R. Soc. London **273**, 247 (1963).
[16] F. Lefloch, J. Hammann, M. Ocio, and E. Vincent, Physica B **203**, 63 (1994).
[17] A. Berton *et al.*, J. Appl. Phys. **52**, 1763 (1981).
[18] H. Takayama, Prog. Theor. Phys. **80**, 827 (1988); J. Phys. Soc. Jpn. **61**, 2512 (1992).
[19] G. Aeppli, S.M. Shapiro, R.J. Birgeneau, and H.S. Chen, Phys. Rev. B **28**, 5160 (1983).
[20] F. Matsubara, T. Tamiya, and T. Shirakura (unpublished).
[21] S. Basu and S.K. Ghatak, J. Magn. Magn. Mater. **123**, 97 (1993).
[22] F. Aguilera-Granja (private communication).